Influence of ferromagnetic walls on resistive wall mode stability in tokamaks

2014 Plasma Phys. Control. Fusion 56 105002

(http://iopscience.iop.org/0741-3335/56/10/105002)

IOP Publishing Plasma Physics and Controlled Fusion

Plasma Phys. Control. Fusion **56** (2014) 105002 (6pp) doi:10.1088/0741-3335/56/10/105002

Influence of ferromagnetic walls on resistive wall mode stability in tokamaks

R Fitzpatrick

Institute for Fusion Studies, Department of Physics, University of Texas at Austin, Austin, TX 78712, USA

E-mail: rfitzp@farside.ph.utexas.edu

Received 8 April 2014, revised 28 July 2014
Accepted for publication 4 August 2014
Published 27 August 2014

Abstract

The effect of a ferromagnetic wall on the stability of the resistive wall mode (RWM) in a tokamak is calculated using a simple quasi-cylindrical plasma model in which the dissipation required to stabilize the mode (in combination with toroidal plasma rotation) is provided by neoclassical poloidal flow damping. For present-day tokamaks, which possess relatively thin walls, ferromagnetism is found to have relatively little influence on the critical toroidal plasma rotation velocity above which the RWM is stabilized, which is almost the same as that calculated for a non-ferromagnetic wall. The same is true for walls of moderate thickness. In fact, ferromagnetism is only found to have a significant effect on the critical velocity in the limit of extreme wall thickness (i.e., a wall thickness comparable with the wall minor radius), in which case increasing wall permeability leads to a marked increase in the critical velocity.

Keywords: resistive wall mode, tokamak, ferromagnetic

1. Introduction

The promising 'advanced tokamak' (AT) concept is only economically attractive provided that the ideal external-kink β-limit [1] is raised substantially in the presence of a rigid, close-fitting, electrically conducting, wall [2–4]. This, in turn, is only possible provided that the so-called resistive wall mode (RWM) is somehow stabilized [5, 6], or controlled [7, 8]. Early (i.e., prior to 2010) tokamak experiments established that RWM stabilization above the ideal no-wall stability limit can be understood as a combined effect of plasma rotational inertia and plasma dissipation [9–11]. Experiments conducted in the previous five years have validated this theory [12–14]. In addition, however, these experiments have provided a much better understanding of the somewhat complex phenomenology of RWM stability in the presence of plasma rotation, especially the destabilization of the mode at moderately high levels of rotation.

In tokamak experiments, the role of the stabilizing wall is played by special electrically-conducting 'passive plates' and/or by the vacuum vessel. These conducting structures are fabricated from a non-ferromagnetic metal such as copper, stainless steel, or Inconel. Up to now, it has been standard practice to avoid (whenever possible) incorporating ferromagnetic materials into tokamaks; firstly, because the magnetic fields generated by such materials greatly complicate plasma control; and, secondly, because ferromagnetic materials are known to destabilize ideal external-kink modes (and other magnetohydrodynamical (MHD) instabilities) [15]. However, economic and environmental considerations in future tokamak reactors demand that the amount of radioactive waste be kept to an absolute minimum. Hence, it is vitally important that the first wall and blanket, which will play the role of the wall in such devices, be fabricated from a low-activation material. Unfortunately, all of the most promising candidate materials, such as F82H steel [16], are ferromagnetic. The likely need to use ferromagnetic walls in fusion reactors has spurred a great deal of recent experimental [17–21] and theoretical [22–27] research into the effect of such walls on RWMs (and other MHD instabilities) in tokamaks. The majority of existing theoretical studies have concentrated on the effect of a ferromagnetic wall on the RWM growth-rate. However, as soon as we accept that any conceivable RWM growth-rate would allow such a mode to grow to a dangerous amplitude in a time that is much less than the lifetime of the plasma discharge, it becomes clear that the central question is the effect of a ferromagnetic wall on the RWM *stability boundaries*. In other words, the central question is the extent to

which a ferromagnetic wall facilitates, or impedes, the ability of modest levels of plasma toroidal rotation to stabilize the RWM, and, thereby, raise the effective β-limit. The aim of this paper is to address this question directly using a relatively simple quasi-cylindrical plasma model in which the dissipation required to stabilize the mode is provided by *neoclassical poloidal flow damping* [28–31].

The neoclassical damping model employed in this paper was selected because it is extremely simple (which is an important consideration, given that the stability diagrams that are shown in figures 1–3 required hundreds of solutions of the RWM dispersion relation), and yet leads to RWM stability boundaries that are broadly consistent with those observed in tokamaks. In recent years, various researchers have developed a drift-kinetic damping model for the RWM [11, 32, 33]. This model, which is significantly more complicated than the neoclassical damping model, has been highly successful at explaining the RWM stability boundaries observed in NSTX [12, 13, 34] and DIII-D [14]. It is interesting to note that the drift-kinetic damping model leads to a cubic dispersion relation (with two roots rotating with the plasma, one leading and one lagging, and one slowly rotating root that can be identified as the RWM) [35, 36], in accordance with results obtained using simple damping models [37] (including the model adopted in this paper—we do not mention the rotating roots, because they are always stable). This encourages us to hope that the conclusions of this paper are generic in nature, rather than being specific to the adopted damping model.

2. Derivation of RWM dispersion relation

2.1. Plasma model

Consider a large aspect-ratio, low-β, circular cross-section tokamak plasma of major radius R_0, minor radius a, on-axis toroidal magnetic field-strength B_0, and on-axis plasma mass density ρ_0. The inverse aspect-ratio of the plasma is $\epsilon_0 = a/R_0$.

In the following, all lengths are normalized to a, all magnetic field-strengths to B_0, and all times to the hydromagnetic time-scale $\tau_{\rm H} = (R_0/B_0)\,\sqrt{\mu_0\,\rho_0}$.

The plasma equilibrium is described by the model safety-factor profile

$$q(r) \equiv \frac{r\,\epsilon_0}{B_\theta(r)} = \frac{q_a\,r^{\,2}}{1-(1-r^{\,2})^{\,q_a/q_0}}, \tag{1}$$

and the model density profile

$$\rho(r) = (1-r^{\,2})^{\,\alpha}. \tag{2}$$

Here, r is the radial distance from the magnetic axis, q_a the safety factor at the edge of the plasma, and q_0 the safety factor on the magnetic axis.

In a large aspect-ratio (i.e., $\epsilon_0 \ll 1$), low-β (i.e., $\beta \lesssim \epsilon_0^2$) tokamak equilibrium, the plasma response to the helical magnetic perturbation generated by a RWM (with, say, m periods in the poloidal direction, and n periods in the toroidal direction) is governed by the eigenmode equation [28–31]

$$r\,\frac{\mathrm{d}}{\mathrm{d}r}\left[\left(\rho\,\gamma'^{\,2}\left[1+\frac{q^2}{\epsilon_0^2}\,\frac{\mu_\parallel}{\gamma'+\mu_\parallel\,r^2}\right]+Q^{\,2}\right)r\,\frac{\mathrm{d}\phi}{\mathrm{d}r}\right] - \left[m^2\left(\rho\,\gamma'\left[\gamma'+\frac{q^2}{\epsilon_0^2}\,\mu_\parallel\right]+Q^{\,2}\right)+r\,\frac{\mathrm{d}Q^{\,2}}{\mathrm{d}r}\right]\phi = 0, \tag{3}$$

where $\gamma' = \gamma - \mathrm{i}\,n\,\Omega_\phi$ is the mode growth-rate in the plasma frame, γ the growth-rate in the laboratory frame, and Ω_ϕ the equilibrium plasma toroidal angular rotation velocity. (Any equilibrium plasma poloidal rotation is neglected in this paper, for the sake of simplicity. Likewise, Ω_ϕ is assumed to be uniform.) Furthermore, $Q(r) = m/q(r) - n$, and $-\gamma'\,\phi$ is the perturbed scalar electric potential associated with the RWM. It is assumed that $m \gg n\,\epsilon_0$. Finally, $\mu_\parallel$ is the *parallel ion viscosity* that ultimately causes neoclassical poloidal flow damping [28–31]. Note that the dissipation due to neoclassical poloidal flow damping is strongly peaked at the edge of the plasma (where Q is small—see the following paragraph). Hence, it is a reasonable approximation to set the neoclassical viscosity profile in equation (3) to a uniform value characteristic of the viscosity at the plasma edge [29].

It is important to note that, in this simple, low-β, quasi-cylindrical model, the m, n ideal external-kink mode (and, hence, the associated RWM) is driven unstable by current gradients, rather than by pressure gradients. Moreover, the mode is only unstable when the associated rational surface (at which $q(r) = m/n$) lies just outside the edge of the plasma: i.e., when the plasma edge is nearly resonant. (Hence, in this paper, q_a is given the value 2.93 to ensure that the $q = 3$ surface lies just outside the edge of the plasma.) The dissipation that occurs in the near-resonant edge region is ultimately responsible for stabilizing the RWM. Of course, in more realistic models, the dissipation that is responsible for stabilizing the RWM takes place at resonant surfaces internal to the plasma.

Launching a well-behaved solution of equation (3) from the magnetic axis ($r = 0$), and integrating to the edge of the plasma ($r = 1$), we obtain the complex *plasma response parameter*

$$s(\gamma) = -\frac{1}{2}\left[1+m^{-1}\,\frac{\mathrm{d}\ln(Q\,\phi)}{\mathrm{d}\ln r}\right]_{r=1}. \tag{4}$$

This parameter fully specifies the response of the plasma to the RWM.

2.2. Plasma stability parameter

The *marginally-stable ideal eigenmode equation*,

$$r\,\frac{\mathrm{d}}{\mathrm{d}r}\left(Q^{\,2}\,r\,\frac{\mathrm{d}\phi}{\mathrm{d}r}\right)-\left(m^2\,Q^{\,2}+r\,\frac{\mathrm{d}Q^{\,2}}{\mathrm{d}r}\right)\phi = 0, \tag{5}$$

is obtained from equation (3) by neglecting plasma inertia, and governs the stability of the ideal external-kink mode [38]. Calculating the plasma response parameter (4) from the above equation, we obtain a real number, $s_{\rm b}$, which is equivalent to the well-known Boozer stability parameter for the ideal external-kink mode [39].

2.3. Vacuum solution

Suppose that the region external to the plasma (i.e., $r > 1$) is bisected by a uniform, rigid, wall (concentric with the edge of the plasma), of (uniform) electrical conductivity σ_w, and (uniform) magnetic permeability μ_w, whose inner and outer surfaces correspond to $r = r_1$ and $r = r_2$, respectively (where $1 < r_1 < r_2$). Let $\psi = Q\,\phi$ be the perturbed poloidal magnetic flux associated with the RMP. Repeating the analysis of section II.C of [31], we find that

$$-m^{-1}\left.\frac{\mathrm{d}\ln\psi}{\mathrm{d}\ln r}\right|_{r=r_{1-}} = \frac{2\,s}{c_1-(1-c_1)\,s}+1, \tag{6}$$

and

$$-m^{-1}\left.\frac{\mathrm{d}\ln\psi}{\mathrm{d}\ln r}\right|_{r=r_{2+}} = 1, \tag{7}$$

where

$$c_1 = r_1^{-2\,m}. \tag{8}$$

2.4. Wall solution

Repeating the analysis of section II.D of [31] (replacing μ_0 by μ_w), we find that

$$-m^{-1}\frac{\mathrm{d}\ln\psi}{\mathrm{d}\ln r} = \frac{p\,r}{m}\,\frac{E\,K_{m-1}(p\,r)-D\,I_{m-1}(p\,r)}{E\,K_m(p\,r)+D\,I_m(p\,r)}+1 \tag{9}$$

within the wall, where $p = (\gamma\,\mu_w\,\sigma_w)^{1/2}$, and E and D are arbitrary constants. Here, $I_m(z)$ and $K_m(z)$ are modified Bessel functions.

2.5. RWM dispersion relation

The matching conditions at the wall's inner and outer boundaries are

$$\left.\frac{\mathrm{d}\ln\psi}{\mathrm{d}\ln r}\right|_{r=r_{1-}} = \frac{1}{\hat{\mu}_w}\left.\frac{\mathrm{d}\ln\psi}{\mathrm{d}\ln r}\right|_{r=r_{1+}}, \tag{10}$$

and

$$\frac{1}{\hat{\mu}_w}\left.\frac{\mathrm{d}\ln\psi}{\mathrm{d}\ln r}\right|_{r=r_{2-}} = \left.\frac{\mathrm{d}\ln\psi}{\mathrm{d}\ln r}\right|_{r=r_{2+}}, \tag{11}$$

respectively, where $\hat{\mu}_w = \mu_w/\mu_0$ is the relative magnetic permeability of the wall. Making use of Equations (6), (7), and (9), we obtain the RWM dispersion relation

$$\frac{\hat{\mu}_w\,s(\gamma)}{c_1-(1-c_1)\,s(\gamma)} = \frac{P}{Q}, \tag{12}$$

where

$$\begin{aligned} P &= y_1\,y_2\left[I_{m-1}(z_2)\,K_{m-1}(z_1)-K_{m-1}(z_2)\,I_{m-1}(z_1)\right]\\ &\quad + y_1\,k\left[I_m(z_2)\,K_{m-1}(z_1)+K_m(z_2)\,I_{m-1}(z_1)\right]\\ &\quad - y_2\,k\left[I_{m-1}(z_2)\,K_m(z_1)+K_{m-1}(z_2)\,I_m(z_1)\right]\\ &\quad - k^2\left[I_m(z_2)\,K_m(z_1)-K_m(z_2)\,I_m(z_1)\right], \end{aligned} \tag{13}$$

$$\begin{aligned} Q &= y_2\left[I_{m-1}(z_2)\,K_m(z_1)+K_{m-1}(z_2)\,I_m(z_1)\right]\\ &\quad + k\left[I_m(z_2)\,K_m(z_1)-K_m(z_2)\,I_m(z_1)\right], \end{aligned} \tag{14}$$

and

$$z_1 = p\,r_1 = \left(2\,m\,\frac{\gamma}{\gamma_w}\,\frac{\hat{\mu}_w}{\epsilon_w}\right)^{1/2}, \tag{15}$$

$$z_2 = p\,r_2 = z_1\,(1+\epsilon_w), \tag{16}$$

with $y_1 = z_1/(2\,m)$, $y_2 = z_2/(2\,m)$, and $k = (\hat{\mu}_w-1)/2$. Here,

$$\gamma_w = \frac{2\,m}{\sigma_w\,r_1\,(r_2-r_1)} \tag{17}$$

is a typical (normalized) RWM growth-rate, and

$$\epsilon_w = \frac{r_2-r_1}{r_1} \tag{18}$$

is a measure of the relative wall thickness.

2.6. Ideal stability boundaries

In the limit $|z_1|/m \to 0$, the dispersion relation (12) yields $s \to s_0$, where

$$s_0 = -\frac{k_+\,k_-\,(c_1-c_2)}{1+k_+\,k_-\,(c_1-c_2)+k_-^2\,(1-c_2/c_1)}, \tag{19}$$

and

$$k_\pm = \frac{\hat{\mu}_w\pm 1}{2\,\hat{\mu}_w^{1/2}}, \tag{20}$$

with $c_2 = r_2^{-2\,m}$. On the other hand, in the limit $|z_1|/m \to \infty$, the dispersion relation gives $s \to s_\infty$, where

$$s_\infty = \frac{c_1}{1-c_1}. \tag{21}$$

It can be shown that $s_b = s_0$ corresponds to the *ideal non-conducting wall stability boundary*: i.e., the stability boundary for the ideal external-kink mode in the limit that the wall is non-conducting (but still ferromagnetic). To be more exact, the ideal mode is stable in the presence of a non-conducting wall (i.e., $\sigma_w \to 0$, which implies that $|z_1|/m \to 0$) when $s_b < s_0$, and unstable otherwise. It can also be shown that $s_b = s_\infty$ corresponds to the *ideal perfectly-conducting wall stability boundary*: i.e., the stability boundary for the ideal external-kink mode in the limit that the wall is perfectly-conducting (and also ferromagnetic). To be more exact, the ideal mode is stable in the presence of a perfectly-conducting wall (i.e., $\sigma_w \to \infty$, which implies that $|z_1|/m \to \infty$) when $s_b < s_\infty$, and unstable otherwise. It is apparent that s_0 becomes more negative as $\hat{\mu}_w$ increases: i.e., in the presence of a non-conducting wall, the ideal external-kink mode is destabilized by increasing wall ferromagnetism. On the other hand, s_∞ is independent of $\hat{\mu}_w$: i.e., in the presence of a perfectly-conducting wall, the ideal external-kink mode is unaffected by wall ferromagnetism.

As is well known for the model used here, the ideal non-conducting wall stability boundary, $s_b = s_0$, corresponds to the RWM stability boundary in the absence of plasma rotation [29–31]. Thus, equation (19) implies that the ferromagnetic destabilization of the RWM in the absence of plasma rotation is insignificant when $k_-\,(c_2-c_1) \sim (\hat{\mu}_w-1)\,(r_2-r_1) \ll 1$. Now, we expect a ferromagnetic wall to be largely saturated by the strong toroidal magnetic field that is always present

in tokamaks, which implies that $\hat{\mu}_w - 1 \sim \mathcal{O}(1)$ [40]. Hence, we deduce that any ferromagnetic destabilization of the RWM is insignificant unless the wall is radially thick: i.e., unless $r_2 - r_1 \sim \mathcal{O}(1)$ [25]. It follows that experimental demonstrations that radially thin ferromagnetic walls have little or no discernable effect on RWM stability in tokamaks [17, 18, 20] are not necessarily definitive, because the walls in fusion reactors will, almost certainly, be thick. On the other hand, it is clear that ferromagnetism from a thick wall will have a negative impact on RWM stability.

Finally, it is helpful to define the real *plasma stability parameter*:

$$\bar{s} = \frac{s_b - s_0}{s_\infty - s_0}. \tag{22}$$

The ideal non-conducting wall stability limit corresponds to $\bar{s} = 0$, whereas the ideal perfectly-conducting wall stability limit corresponds to $\bar{s} = 1$.

3. Numerical results

3.1. Calculation parameters

The calculations described in this paper were all performed using parameters appropriate to a predominately $m = 3$, $n = 1$ RWM in a typical DIII-D plasma. The DIII-D tokamak has major radius $R_0 = 1.69\,\mathrm{m}$, minor radius $a = 0.61$ m, typical on-axis toroidal field-strength $B_0 = 2.1\,\mathrm{T}$, and typical on-axis electron number density $n_0 = 6 \times 10^{19}\,\mathrm{m}^{-3}$ [41]. It follows that $\tau_H = 3 \times 10^{-7}\,\mathrm{s}$. The typical electron number density, electron temperature, and ion temperature at the edge of a DIII-D discharge are $n_e = 2 \times 10^{19}\,\mathrm{m}^{-3}$, $T_e = 100\,\mathrm{eV}$, and $T_i = 100\,\mathrm{eV}$, respectively [42]. This implies that $\mu_\parallel = 1 \times 10^{-4}$ (in normalized units) [30].

In DIII-D, the Inconel vacuum vessel serves as the conducting structure for kink/ballooning mode stabilization. Henceforth, we shall refer to this structure as the 'DIII-D wall'. The DIII-D wall parameters, c_1 and γ_w, were determined by fitting to data obtained from the VALEN code [43], which calculates the RWM growth-rate as a function of the Boozer stability parameter, s_b, for a dissipationless plasma, and accurately models the DIII-D wall in three-dimensions via a finite-element representation that employs a standard thin-shell integral formulation. The fitting procedure (which was performed for a predominately 3, 1 mode) yields $c_1 = 0.14$ and $\gamma_w = 8 \times 10^{-5}$ (in normalized units) [30].

According to equation (8), the effective radius of the DIII-D wall (for an 3, 1 RWM) is $r_1 = c_1^{-1/6} = 1.39$ (in normalized units). Given that the wall is fabricated from Inconel 625 [44], which has an electrical resistivity of $\eta_w = \sigma_w^{-1} = 1.26 \times 10^{-6}\,\Omega\,\mathrm{m}$, it follows from equation (17) that $\gamma_w = 3.5 \times 10^{-6}\,(r_2 - r_1)^{-1}$ (in normalized units), which implies that the effective thickness of the wall is $r_2 - r_1 = 4.4 \times 10^{-2}$ (in normalized units). Hence, from equation (18), the appropriate wall thickness parameter for a 3, 1 RWM in a DIII-D plasma is $\epsilon_w = 3.2 \times 10^{-2}$.

The stability boundaries for a 3, 1 RWM in a DIII-D discharge were determined numerically by adjusting the central safety-factor, q_0, and the (normalized) plasma toroidal angular velocity Ω_ϕ, until the RWM dispersion relation (12) yielded a purely imaginary growth-rate. To be more exact, a Newton iteration search algorithm was executed in q_0–Ω_ϕ space until the real part of the RWM growth-rate was zero. The stability boundaries were mapped by varying the starting point of this search algorithm in q_0–Ω_ϕ space. The values of q_0 corresponding to the stability boundaries shown in figures 1–3 lie in the range 1.18 to 1.27.

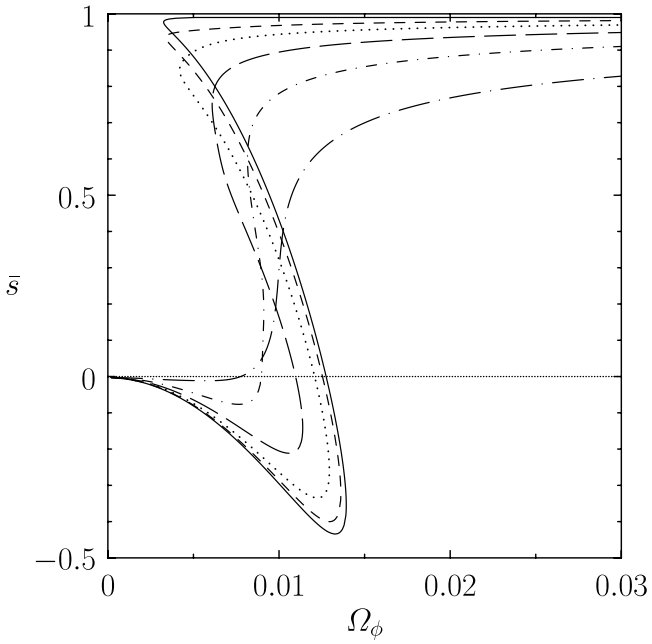

Figure 1. RWM stability boundary plotted in normalized plasma toroidal angular velocity versus ideal plasma stability space. The RWM is unstable at all points in $\Omega_\phi - \bar{s}$ space that lie either to the left of or above the stability boundary, and is stable otherwise. The calculation parameters are $m = 3$, $n = 1$, $\alpha = 0.5$, $q_a = 2.93$, $\epsilon_0 = 0.32$, $\mu_\parallel = 1 \times 10^{-4}$, $c_1 = 0.14$, $\gamma_w = 8 \times 10^{-5}$, and $\hat{\mu}_w = 2$. The solid, dashed, dotted, long-dashed, dashed–dotted, and long-dashed–dotted curves correspond to $\epsilon_w = 10^{-3}$, 10^{-2}, $10^{-3/2}$, 10^{-1}, $10^{-1/2}$, and 10^{+0}, respectively. The ideal perfectly-conducting wall stability boundary lies at $\bar{s} = 1$, which corresponds to $s_b = 0.163$ in all cases. The ideal non-conducting wall stability boundary lies at $\bar{s} = 0$, which corresponds to $s_b = -3.14 \times 10^{-4}$, -3.01×10^{-3}, -8.68×10^{-3}, -2.12×10^{-2}, -3.71×10^{-2}, and -4.40×10^{-2}, respectively.

3.2. Results

Figure 1 shows the calculated stability boundary of the 3, 1 RWM in a typical DIII-D plasma, plotted in ideal plasma stability, $\bar{s}$, versus normalized plasma toroidal angular velocity, Ω_ϕ, space, for a relative wall permeability of $\hat{\mu}_w = 2$, and various different values of the wall thickness parameter, ϵ_w. Note that varying ϵ_w, while keeping γ_w fixed, is equivalent to replacing the DIII-D wall with one of a different thickness that possesses the same overall electrical resistance. The fact that $\hat{\mu}_w > 1$ implies that the replacement wall is also significantly ferromagnetic.

The solid curve corresponds to the thin ferromagnetic wall limit. It can be seen that for this model, and in this limit, in which we would not expect ferromagnetism to modify

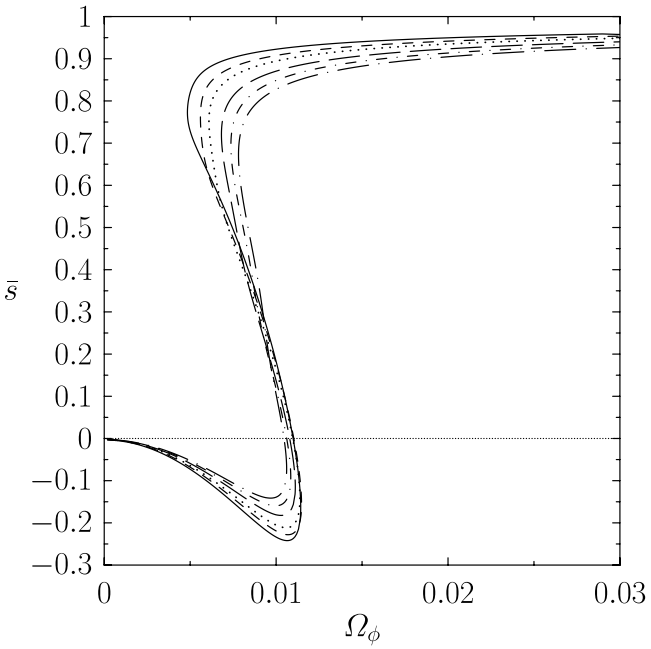

Figure 2. RWM stability boundary plotted in normalized plasma toroidal angular velocity versus ideal plasma stability space. The calculation parameters are $m = 3$, $n = 1$, $\alpha = 0.5$, $q_a = 2.93$, $\epsilon_0 = 0.32$, $\mu_\parallel = 1 \times 10^{-4}$, $c_1 = 0.14$, $\gamma_w = 8 \times 10^{-5}$, and $\epsilon_w = 0.1$. The solid, dashed, dotted, long-dashed, dashed–dotted, and long-dashed–dotted curves correspond to $\hat{\mu}_w = 1.0$, 1.5, 2.0, 3.0, 4.0, and 5.0, respectively. The ideal perfectly-conducting wall stability boundary lies at $\bar{s} = 1$, which corresponds to $s_b = 0.163$ in all cases. The ideal non-conducting wall stability boundary lies at $\bar{s} = 0$, which corresponds to $s_b = 0$, -1.23×10^{-2}, -2.12×10^{-2}, -3.43×10^{-2}, -4.39×10^{-2}, and -5.15×10^{-2}, respectively.

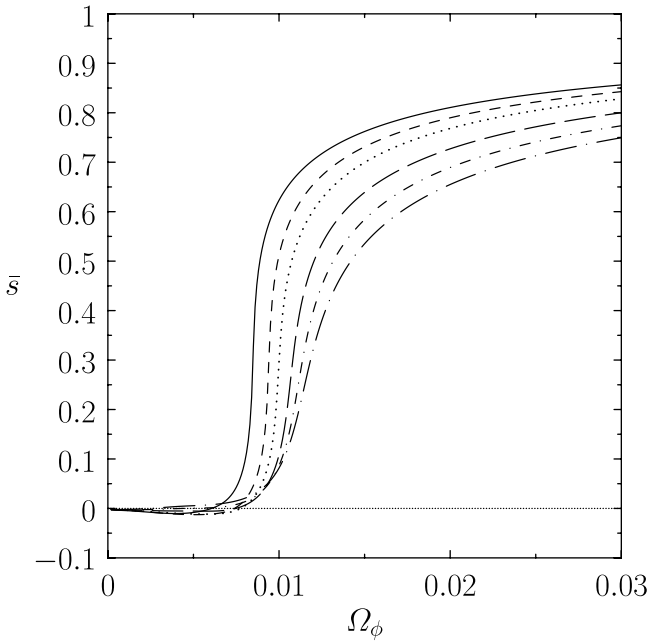

Figure 3. RWM stability boundary plotted in normalized plasma toroidal angular velocity versus ideal plasma stability space. The calculation parameters are $m = 3$, $n = 1$, $\alpha = 0.5$, $q_a = 2.93$, $\epsilon_0 = 0.32$, $\mu_\parallel = 1 \times 10^{-4}$, $c_1 = 0.14$, $\gamma_w = 8 \times 10^{-5}$, and $\epsilon_w = 1.0$. The solid, dashed, dotted, long-dashed, dashed–dotted, and long-dashed–dotted curves correspond to $\hat{\mu}_w = 1.0$, 1.5, 2.0, 3.0, 4.0, and 5.0, respectively. The ideal perfectly-conducting wall stability boundary lies at $\bar{s} = 1$, which corresponds to $s_b = 0.163$ in all cases. The ideal non-conducting wall stability boundary lies at $\bar{s} = 0.$, which corresponds to $s_b = 0$, -2.68×10^{-2}, -4.40×10^{-2}, -6.47×10^{-2}, -7.68×10^{-2}, and -8.47×10^{-2}, respectively.

the RWM stability boundary, the RWM is stabilized once the plasma toroidal rotation velocity is sufficiently large. Moreover, this stabilization extends almost all of the way to the perfect-wall stability boundary, $\bar{s} = 1$, which implies that the effective β-limit of the rotationally stabilized plasma is the perfect-wall β-limit.

The dotted curve corresponds to a ferromagnetic wall that has the same thickness as the DIII-D wall. It can be seen that the finite wall thickness makes very little difference to the RWM stability boundary, which is almost the same as that calculated in the thin-wall limit. This suggests that the conventional thin-wall approximation is perfectly adequate for calculating RWM stability boundaries in present-day tokamaks [31], and also that ferromagnetic effects in walls whose thicknesses are similar to those of present-day tokamaks are likely to make very little difference to RWM stability boundaries.

The long-dashed, dashed–dotted, and long-dashed–dotted curves correspond to ferromagnetic walls that are much thicker than the DIII-D wall (but have the same electrical resistance). It can be seen that, close to the no-wall stability boundary, $\bar{s} = 0$, the critical plasma toroidal rotation velocity needed to stabilize the RWM is reduced in the presence of a thick wall (relative to that needed to stabilize the mode in the presence of thin wall of the same electrical resistance and relative permeability). On the other hand, close to the perfect-wall stability boundary, $\bar{s} = 1$, the critical rotation velocity is increased in the presence of a thick wall. In fact, it is clear from the figure that a thick wall significantly impedes the ability of plasma rotation to stabilize the RWM all the way to the perfect-wall stability boundary. This suggests that the effective β-limit for a plasma in which the RWM is rotationally stabilized is significantly lower in the presence of a thick wall, relative to that in the presence of a thin wall of the same electrical resistance and relative permeability [31].

Figure 2 shows the stability boundary of the 3, 1 RWM in a typical DIII-D plasma, calculated for a series of walls of moderate thickness (i.e., $\epsilon_w = 0.1$), and various different values of the relative permeability, $\hat{\mu}_w$. It can be seen that, while increasing wall permeability destabilizes the RWM in the absence of plasma rotation (in other words, the critical value of the Boozer stability parameter, s_b, above which the mode is destabilized, in the absence of plasma rotation, decreases with increasing wall permeability), it has very little effect on the critical plasma toroidal rotation velocity above which the mode is stabilized, which is almost the same as that calculated for a non-ferromagnetic wall.

Finally, figure 3 shows the stability boundary of the 3, 1 RWM in a typical DIII-D plasma, calculated for a series of walls of extreme thickness (i.e., $\epsilon_w = 1.0$), and various different values of the relative permeability, $\hat{\mu}_w$. In can be seen that, in this case, increasing wall permeability leads to a significant increase in the critical plasma toroidal rotation velocity above which the RWM is stabilized, and also impedes the ability of plasma rotation to stabilize the mode all the way to the perfect-wall stability boundary.

4. Summary

We have determined the effect of a ferromagnetic wall on the stability of the RWM in a tokamak using a previously published [28–31] quasi-cylindrical plasma model in which the dissipation required to stabilize the mode (in combination with plasma toroidal rotation) is provided by neoclassical poloidal flow damping. It is assumed that the wall is largely saturated by the strong toroidal magnetic field that is always present in tokamaks, so that its relative permeability does not greatly exceed unity. We find that for present-day tokamaks, such as DIII-D, which possess relatively thin walls, ferromagnetism has relatively little influence on the critical plasma toroidal rotation velocity above which the RWM is stabilized, which is almost the same as that calculated for a non-ferromagnetic wall. The same is true for walls of moderate thickness. In fact, ferromagnetism only has a significant effect on the critical velocity in the limit of extreme wall thickness (i.e., a wall thickness comparable with the wall minor radius), in which case increasing wall permeability leads to a marked increase in the critical velocity, and also greatly impedes the ability of plasma rotation to stabilize the mode all the way to the perfect-wall stability boundary.

Acknowledgment

This research was funded by the US Department of Energy under contract DE-FG02-04ER-54742.

References

[1] Troyon F, Gruber R, Saurenmann H, Semenzato S and Succi S 1984 *Plasma Phys. Control. Fusion* **26** 209
[2] Kessel C, Manickam J, Rewoldt G and Tang W M 1994 *Phys. Rev. Lett.* **72** 1212
[3] Strait E J *et al* 1995 *Phys. Rev. Lett.* **46** 2483
[4] Lazarus E A *et al* 1996 *Phys. Rev. Lett.* **77** 2714
[5] Goedbloed J P, Pfirsch D and Tasso H 1972 *Nucl. Fusion* **12** 649
[6] Sabbagh S A *et al* 2006 *Nucl. Fusion* **46** 635
[7] Okabayashi M *et al* 2005 *Nucl. Fusion* **45** 1715
[8] Sabbagh S A *et al* 2006 *Phys. Rev. Lett.* **97** 045004
[9] Bondeson A and Ward D J 1994 *Phys. Rev. Lett.* **72** 2709
[10] Betti R and Freidberg J P 1995 *Phys. Rev. Lett.* **74** 2949
[11] Hu B and Betti R 2004 *Phys. Rev. Lett.* **93** 105002
[12] Sabbagh S A *et al* 2010 *Nucl. Fusion* **50** 025020
[13] Berkery J W *et al* 2010 *Phys. Rev. Lett.* **104** 035003
[14] Reimerdes H *et al* 2011 *Phys. Rev. Lett.* **106** 215002
[15] Gimblett C 1986 *Nucl. Fusion* **26** 617
[16] Tamura M, Hayakawa H, Yoshitake A, Hishinuma A and Kondo T 1988 *J. Nucl. Mater.* **155–157** 620
[17] Nakayama T, Abe M, Tadokoro T and Otsuka M 1999 *J. Nucl. Mater.* **271–272** 491
[18] Tsuzuki K *et al* 2003 *Nucl. Fusion* **43** 1288
[19] Bakhtiari M *et al* 2003 *Phys. Plasmas* **10** 3212
[20] Tsuzuki K *et al* 2006 *Nucl. Fusion* **46** 966
[21] Bergerson W F *et al* 2008 *Phys. Rev. Lett.* **101** 235005
[22] Kurita G *et al* 2003 *Nucl. Fusion* **43** 949
[23] Kurita G *et al* 2006 *Nucl. Fusion* **46** 383
[24] Akutsu T and Fukuyama A 2006 *Plasma Phys. Control. Fusion* **48** 635
[25] Pustovitov V D 2009 *Phys. Plasmas* **16** 052503
[26] Pustovitov V D, Villone F and JET-EFDA contributers 2010 *Plasma Phys. Control. Fusion* **52** 065010
[27] Pustovitov V D and Yanovskiy V V 2014 *Phys. Plasmas* **21** 022516
[28] Shaing K C 2004 *Phys. Plasmas* **11** 5525
[29] Fitzpatrick R and Bialek J 2006 *Phys. Plasmas* **13** 072512
[30] Fitzpatrick R 2007 *Phys. Plasmas* **14** 022505
[31] Fitzpatrick R 2012 *Phys. Plasmas* **20** 012504
[32] Bondeson A and Chu M S 1996 *Phys. Plasmas* **3** 3013
[33] Liu Y, Chu M S, Chapman I T and Hender T C 2008 *Phys. Plasmas* **15** 112503
[34] Berkery J W *et al* 2011 *Phys. Rev. Lett.* **106** 075004
[35] Liu Y *et al* 2009 *Phys. Plasmas* **16** 056113
[36] Berkery J W, Betti R and Sabbagh S A 2011 *Phys. Plasmas* **18** 072501
[37] Fitzpatrick R and Aydemir A Y 1996 *Nucl. Fusion* **36** 11
[38] Newcomb W A 1960 *Ann. Phys.* **10** 232
[39] Boozer A H 1998 *Phys. Plasmas* **5** 3350
[40] Shiba K, Hishinuma A, Oyana A and Masamura K 1997 *JAERI-Tech* **97-038**
[41] Remierdes H *et al* 2006 *Phys. Plasmas* **13** 056107
[42] Stacey W M and Groebner R J 2006 *Phys. Plasmas* **13** 012513
[43] Bialek J, Boozer A H, Mauel M E and Navratil G A 2001 *Phys. Plasmas* **8** 2170
[44] Trester P W, Kaae J L and Gallix R 1985 *J. Nucl. Mater.* **133–134** 347